

Isotope Fractionation of Mercury during Its Photochemical Reduction by Low-Molecular-Weight Organic Compounds

Wang Zheng* and Holger Hintelmann

Environmental and Life Sciences Program, Trent University, 1600 West Bank Drive, Peterborough, Ontario K9J 7B8, Canada

Received: November 23, 2009; Revised Manuscript Received: February 15, 2010

Photochemical reduction of Hg(II) by various low-molecular-weight organic compounds (LMWOC) was investigated to evaluate the effect of specific functional groups that are typically encountered in natural dissolved organic matters (DOM) on the photoreactivity and isotope fractionation of Hg. LMWOC with reduced sulfur functional groups (e.g., cysteine, glutathione) resulted in slower photochemical reduction of Hg(II) than those without reduced sulfur groups (e.g., serine, oxalic acid). Reduction rate constants were specifically determined for two contrasting LMWOC: DL-serine (0.640 h^{-1}) and L-cysteine (0.047 h^{-1}). Different mass independent isotope effects of Hg were induced by the two types of LMWOC. S-containing ligands specifically enriched magnetic isotopes (^{199}Hg and ^{201}Hg) in the product (Hg(0)) while sulfurless ligands enriched ^{199}Hg and ^{201}Hg in the reactant (Hg(II)), suggesting that opposite magnetic isotope effects were produced by different types of ligands. The nuclear field shift effect was also observed in the photochemical reduction by serine. These isotope effects are related to specific functional groups and reduction mechanisms, and may be used to distinguish between primary and secondary photochemical reduction mechanisms of Hg(II) and to explain isotope fractionation during the photochemical reduction of Hg(II) by natural DOM, which provides mixed bonding conditions.

1. Introduction

Photochemical reduction of Hg(II) is one of the most important pathways of elemental Hg(0) production in natural waters and therefore plays a key role in Hg(0) emission and bioavailability.¹ However, its mechanism remains in debate. Both direct photolysis of Hg(II)–organic ligands complexes^{2–4} and secondary reduction by the products of primary photochemical processes^{5–8} are proposed to be responsible for photochemical reduction of Hg(II) in natural waters. It is not yet known which mechanism is more dominant in specific situations,^{9,10} but both highlight the importance of organic ligands, which primarily consist of various functional groups of dissolved organic matter (DOM). A large number of studies demonstrated that Hg(II) most strongly binds to reduced sulfur functional groups of DOM, such as thiol, disulfide/disulfane, and thioether, rather than O/N donor groups, such as carboxylic, phenol, and amine groups.^{11–13} Due to different stability and reactivity of different Hg(II)–organic ligand complexes, the mechanism and kinetics of photochemical reduction and accompanied isotope fractionation of Hg could vary dramatically.

Low-molecular-weight organic compounds (LMWOC) ($M_r < \sim 1000$ ^{14,15}) are usually good surrogates for different functional groups of natural DOM in terms of their interaction with metal ions because of their simple, identifiable structure. For example, the stability constants of strong Hg–DOM bonds (e.g., $\log K > 20$) are similar to those between Hg and LMWOC containing reduced sulfur, such as cysteine, glutathione, and thiosalicylic acid,^{16–19} while weaker binding sites have stability constants (e.g., $\log K = \sim 10$) similar to carboxylic and phenolic ligands such as oxalic, citric, and salicylic acids.^{17,18} In natural waters, LMWOC are produced by photodegradation of DOM^{20–23} and

they are known to reduce Hg(II) under UV and visible light.^{24–27} Therefore, LMWOC may contribute a substantial part to the natural photochemical reduction of Hg(II).

Photochemical reduction of Hg(II) by natural DOM was found to generate mass independent isotope fractionation (MIF),²⁸ which attracted attention to anomalous isotope effects of Hg.^{29–35} Recently, Zheng and Hintelmann³⁶ reported a variation of reduction rates and MIF with Hg/DOC ratios during photochemical reduction, suggesting the mechanism of MIF may differ for Hg(II) binding to different binding sites of DOM. Until now, only the overall isotope effect caused by the bulk DOM has been determined. However, it is necessary to understand the contributions of specific binding sites to the overall isotope effects to interpret the mechanisms of photochemical reduction and reactivity of Hg in natural waters. Since LMWOC simulate different binding sites of DOM, photochemical reduction of Hg(II) by LMWOC should reveal specific isotope effects resulting from different binding scenarios with DOM.

Isotope fractionation, especially MIF, is a powerful tool in tracking the pathway of Hg transformations and reaction mechanisms. To date, two MIF mechanisms have been recognized for the Hg isotope system. The nuclear field shift effect (NFS), originating from the size and shape of nuclei, occurs when there are changes in electronic configuration during reactions and tends to enrich smaller/lighter isotopes in substances with higher electron density at the nuclei, which corresponds to more s-orbital electrons or less p, d, and f electrons.^{37,38} NFS has only been observed during evaporation³⁹ and abiotic nonphotochemical reduction of Hg.⁴⁰ The other MIF mechanism is the magnetic isotope effect (MIE), originating from different reaction rates of magnetic and nonmagnetic isotopes during spin-selective reactions. ^{199}Hg and ^{201}Hg have unpaired nuclear spins ($I = 1/2$ for ^{199}Hg and $I = 3/2$ for ^{201}Hg) and are thus subject to MIE. Photolysis is the most studied

* Corresponding author. E-mail: wangzheng@trentu.ca.

reaction that induces MIE because it generates spin-related radical pair cages, which initiate spin-selective recombination or cage escape.^{41,42} MIE was found to enrich magnetic isotopes (e.g., ¹⁹⁹Hg and ²⁰¹Hg) in the initial reactants in most cases.^{41,43–45} However, a few studies also observed the reverse of normal MIE, the depletion of magnetic isotopes in the initial reactants.^{46–49} The diversity of MIF shows great potential in tracking the pathways of Hg transformation but calls for a better understanding on their mechanisms and differences.

In this study, photochemical reduction of Hg(II) by two classes of LMWOC with and without reduced sulfur functional groups was investigated to elucidate the effects of specific functional groups on the reactivity and isotope fractionation of Hg. Mechanisms of photochemical reduction and various mass independent isotope effects are discussed.

2. Methods

2.1. Photochemical Reduction by Serine and Cysteine (Time-Series Experiment). This time-series experiment studies the detailed kinetics and evolution of isotope composition of Hg during photochemical reduction by two contrasting LMWOC: serine and cysteine. They have very similar structures and functional groups except the –OH in serine is replaced with –SH in cysteine. The solutions of LMWOC are prepared by dissolving 400 μmol of DL-serine or L-cysteine (Sigma-Aldrich) in 1 L of deoxygenized Milli-Q water in quartz bottles. All procedures described below were conducted in parallel for these two solutions. They were spiked with inorganic Hg(II) standards (NIST3133, in 0.12 M HCl) to reach an initial concentration of 0.2 μM. This Hg concentration is higher than those found in most natural waters but still gives a stoichiometric ratio LMWOC/Hg of ~2000, which is similar to the low Hg/DOC condition found in natural waters and ensures that the ligands are in large excess of Hg. The initial pH of these solutions is 3.6 for cysteine and 3.8 for serine, similar to the pH of very acidic lakes. A slight variation of pH (±0.1) was observed during the course of experiments. The Hg–LMWOC mixtures were placed in the dark for 14 h, allowing Hg(II) to fully equilibrate with LMWOC. Then, the initial solutions were purged with ultrapure Ar to remove Hg(0) produced during the equilibration period. This portion of Hg(0) was collected in 30 mL of KMnO₄ trapping solution (details of trapping solution as described in Zheng et al.⁵⁰). Next, the quartz reactors containing the Hg–LMWOC solutions were exposed to solar irradiation delivered by a Suntest XLS+ (ATLAS Electric Devices Co.). The solar simulator was equipped with a high-pressure xenon lamp and special UV filter that transmits wavelength between 300–800 nm. The spectrum of the lamp closely resembles the natural sunlight. The light intensity was 700 W/m². The temperature of the quartz reactors was maintained between 293 and 295 K by a circulating water bath. During irradiation, Hg(0) produced was constantly purged with Ar into 800 mL of KMnO₄ trapping solutions. Subsamples were taken from both the quartz reactors, which contain remaining Hg(II) reactant, and the trapping solutions, which contain accumulated Hg(0) product, at certain time intervals. Subsamples were immediately treated with 2% BrCl to quench further reduction and were kept refrigerated.

After irradiation, the quartz reactors were emptied and filled with 1 L of 0.5% BrCl solution to dissolve Hg that may have adsorbed to container walls. This portion of Hg was found to be <0.1% of the initial Hg and was considered negligible.

2.2. Photochemical Reduction by 12 Different LMWOC (Screening Experiment). This experiment is intended to examine the extent of reduction of Hg(II) by a wide range of

LMWOC. Twelve different compounds were examined, consisting of two groups based on the presence or absence of reduced sulfur functional groups. S-containing compounds include cysteine, glutathione, cysteamine, methionine, and thiourea, and sulfurless compounds include oxalic acid, glycolic acid, glycine, ethylene glycol, serine, ethylenediamine, and EDTA. The experimental procedures are similar to the method employed in the time-series experiment. The main differences are (1) the initial concentrations of LMWOC and Hg(II) are lowered to 20 and 0.01 μM but still maintain a LMWOC/Hg ratio of 2000; (2) solutions were prepared in 100 mL of PFA (Teflon) bottles; (3) the initial pH is around 6.0 due to the lower concentration of LMWOC, with ethylenediamine and cysteamine solutions being more alkaline (pH around 8); and (4) the solar irradiation lasted 15 h, and subsamples were only collected at the end of irradiation.

2.3. Analysis of Hg Concentration and Isotope Ratios. Concentrations of total Hg in all subsamples were measured using a Tekran 2600 CV-AFS (Tekran Instruments, Inc.) following EPA method 1631 revision E. Isotope ratios of Hg were measured by multicollector inductively coupled plasma mass spectrometry (MC-ICP/MS, Neptune, Thermo Scientific) using the method described by Zheng and Hintelmann.^{36,40} Briefly, a minimum volume of NH₂OH·HCl (3.1 M, Sigma-Aldrich) was added to all samples to neutralize excessive BrCl and KMnO₄ before analysis. The MC-ICP/MS was coupled to a cold vapor generation system, where Hg(II) was converted to Hg(0) vapor by SnCl₂ (0.16 M, Sigma-Aldrich) and subsequently mixed with Tl aerosol generated by an Apex-Q nebulizer (Elemental Scientific Inc.). Before entering the plasma, the Hg–Tl mixture stream was passed through a Nafion dryer (PERMA PURE), which removed moisture and enhanced the Hg signal. Mass bias was corrected using the ²⁰⁵Tl/²⁰³Tl internal standard and standard bracketing with a 0.01 μM Hg standard (NIST 3133). The concentration and matrix of samples and bracketing standards were matched to within 10%.

Two sets of Faraday cup configurations were used to account for all stable isotopes of Hg and Tl. Set 1 measures ¹⁹⁸Hg, ¹⁹⁹Hg, ²⁰⁰Hg, ²⁰¹Hg, ²⁰²Hg, ²⁰³Tl, and ²⁰⁵Tl, and set 2 measures ¹⁹⁸Hg, ¹⁹⁹Hg, ²⁰¹Hg, ²⁰²Hg, ²⁰⁴Hg, ²⁰³Tl, ²⁰⁵Tl, and ²⁰⁸Pb. All samples from the time-series experiment were measured using set 1. Selected samples were analyzed using set 2 to examine ²⁰⁴Hg. All samples from the screening experiment were measured using set 2.

Isotope compositions are reported using δ values relative to the bracketing standard:

$$\delta^x\text{Hg} = \left(\frac{R_{\text{sample}}^{x/198}}{R_{3133}^{x/198}} - 1 \right) \cdot 1000\text{‰} \quad (1)$$

where $x = 199, 200, 201, 202, 204$. Isotopic anomalies are characterized using the “capital delta” notation (Δ) and is defined as:

$$\Delta^x\text{Hg} = \delta^x\text{Hg} - \frac{\ln(m_{198}/m_x)}{\ln(m_{198}/m_{202})} \times \delta^{202}\text{Hg} \quad (2)$$

where m_x is the atomic mass of isotope x with mass number $x = 199, 200, 201, \text{ and } 204$. The kinetic fractionation factors between product Hg(0) and reactant Hg(II) are determined for the time-series experiment and are defined as $\alpha^{x/198} = R_{\text{product}}/R_{\text{reactant}}$, where R is the isotope ratio of Hg. The following form of the Rayleigh equation was used to evaluate kinetic fractionation factors:

$$\ln \frac{1000 + \delta}{1000 + \delta_0} = (\alpha^{x/198} - 1) \ln f_R \quad (3)$$

where δ is $\delta^x\text{Hg}$ (as defined by eq 1) of reactant Hg(II). δ_0 is the initial δ value of the reactant and f_R is the fraction of residual reactant Hg(II).

The external reproducibility of the method is evaluated using a secondary reference material, the Almadén Hg standard (in 1% BrCl), which was analyzed repeatedly in each analytical session. $\delta^{202}\text{Hg}$, $\Delta^{201}\text{Hg}$, and $\Delta^{199}\text{Hg}$ measured during all analytical sessions are $-0.63 \pm 0.05 \text{‰}$ (2SD, $n = 11$), $-0.02 \pm 0.09 \text{‰}$ (2SD, $n = 11$), and $-0.03 \pm 0.07 \text{‰}$ (2SD, $n = 11$), respectively. Two Almadén standards were measured at a lower concentration ($\sim 1.5 \text{ nM}$) because two samples from the time-series experiment and several samples from the screening experiment were measured at this concentration. Despite lower internal repeatability, $\delta^{202}\text{Hg}$ of these two Almadén standards are -0.59 and -0.61‰ , not different from the average δ of all Almadén standards.

3. Results

3.1. Photochemical Reduction by Serine and Cysteine (Time-Series Experiment). **3.1.1. Reduction Kinetics.** Fractions of Hg of the reactant (f_R) and the product (f_P) are plotted in Figure 1 against time. In the dark, only 0.4% and 0.5% of initial Hg(II) was reduced after 14 h by cysteine and serine, respectively, suggesting reduction in the absence of light is negligible. Under solar irradiation, reduction was significantly enhanced. The reduction by cysteine closely follows a pseudo-first-order rate law: $f_{R_{\text{cys}}} = 0.99e^{-0.047t}$ ($P < 0.0001$ for both coefficients; subscript “cys” denotes cysteine). The reduction by serine is notably faster and also follows a pseudo-first-order rate law ($f_{R_{\text{ser}}} = 1.04e^{-0.640t}$; $P < 0.0001$ for both coefficients; “ser” denotes serine) during the first 4 h. However, after 4 h, the reduction rate slowed down significantly. This may represent a change in reduction mechanisms but may be also due to higher uncertainties of $f_{R_{\text{ser}}}$ related to the low concentration of Hg(II) after 4 h (only 0.3–0.1% of the initial Hg). Generally, the sums of f_P and f_R are in good agreement with the initial Hg.

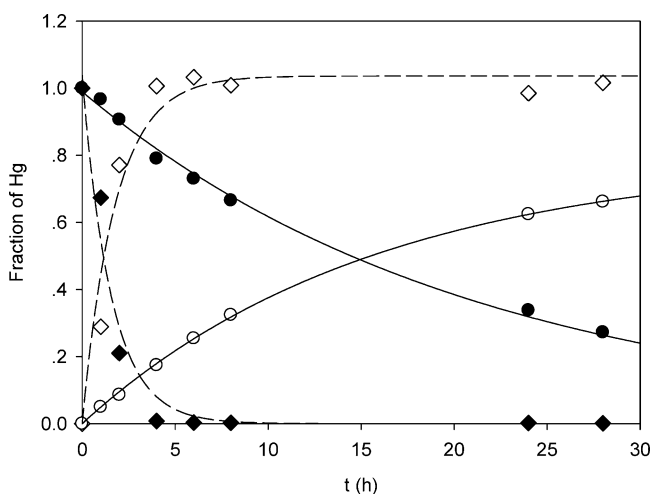


Figure 1. Kinetics of photochemical reduction of Hg(II) by serine and cysteine. Symbols: (●) reactant Hg(II) in reduction by serine, (◇) product Hg(0) in reduction by serine, (●) reactant Hg(II) in reduction by cysteine, (○) product Hg(0) in reduction by cysteine. The solid line and dashed line are pseudo-first-order fits for cysteine and serine, respectively.

TABLE 1: Fractionation Factors of Photochemical Reduction of Hg(II) by Cysteine and Serine (Time-Series Experiment)^a

	$10^3 \ln \alpha^{199}$	$10^3 \ln \alpha^{200}$	$10^3 \ln \alpha^{201}$	$10^3 \ln \alpha^{202}$
cysteine	0.69 ± 0.04	-0.67 ± 0.03	-0.26 ± 0.07	-1.32 ± 0.07
serine	-0.26 ± 0.04	-0.83 ± 0.02	-1.22 ± 0.04	-1.71 ± 0.03

^aUncertainties are 2SE. For serine, only samples collected up to 4 h of irradiation are considered. See text for details.

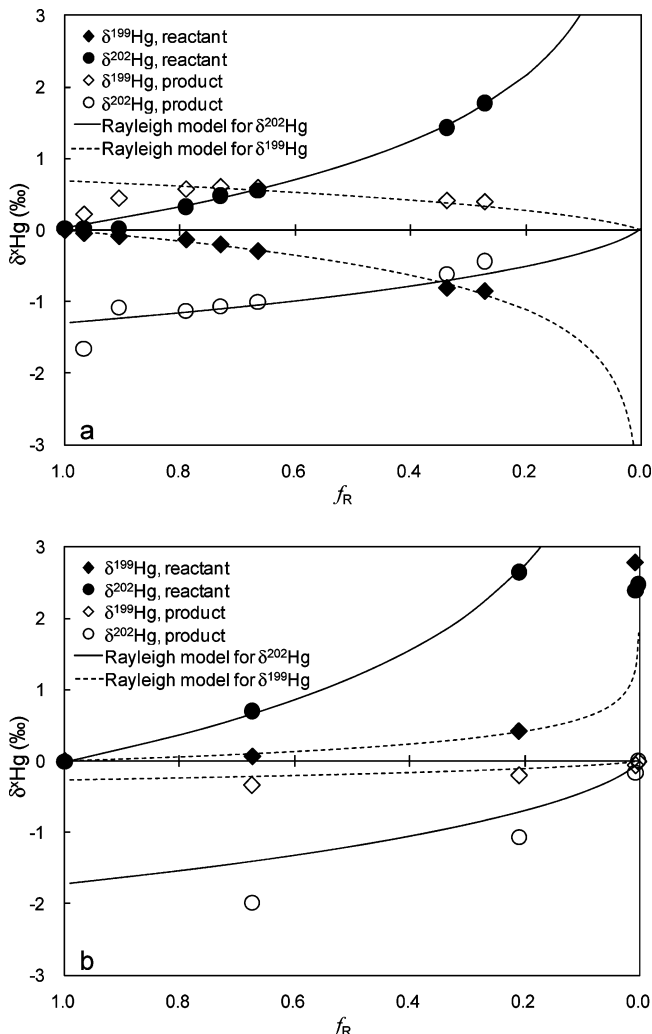


Figure 2. Rayleigh fractionation during photochemical reduction of Hg(II) by cysteine (a) and serine (b). Curves of Rayleigh models are plotted on the basis of the fractionation factors in Table 1.

3.1.2. Isotope Fractionation during Photochemical Reduction by Cysteine. Isotope fractionation factors are listed in Table 1. They are calculated using eq 3, assuming Rayleigh fractionation. Figure 2 shows the evolution of isotope compositions of Hg as a function of the fraction of residual reactant Hg(II). Rayleigh models calculated using fractionation factors listed in Table 1 are fitted to data points. For the reduction by cysteine (Figure 2a), $\delta^{202}\text{Hg}$ of both the reactant and product follow the Rayleigh model well. The heavier isotope (^{202}Hg) was progressively accumulated in the reactant. However, what is surprising in our results is that $\delta^{199}\text{Hg}$ appears to follow a “reversed” Rayleigh model, being consistently negative. The depletion of ^{199}Hg in the reactant is also evident from the positive $10^3 \ln \alpha^{199}$ (Table 1). $\delta^{199}\text{Hg}$ of the product also followed the same “reversed” Rayleigh model. This isotope effect is certainly not mass dependent and is opposite to the known isotope effects of

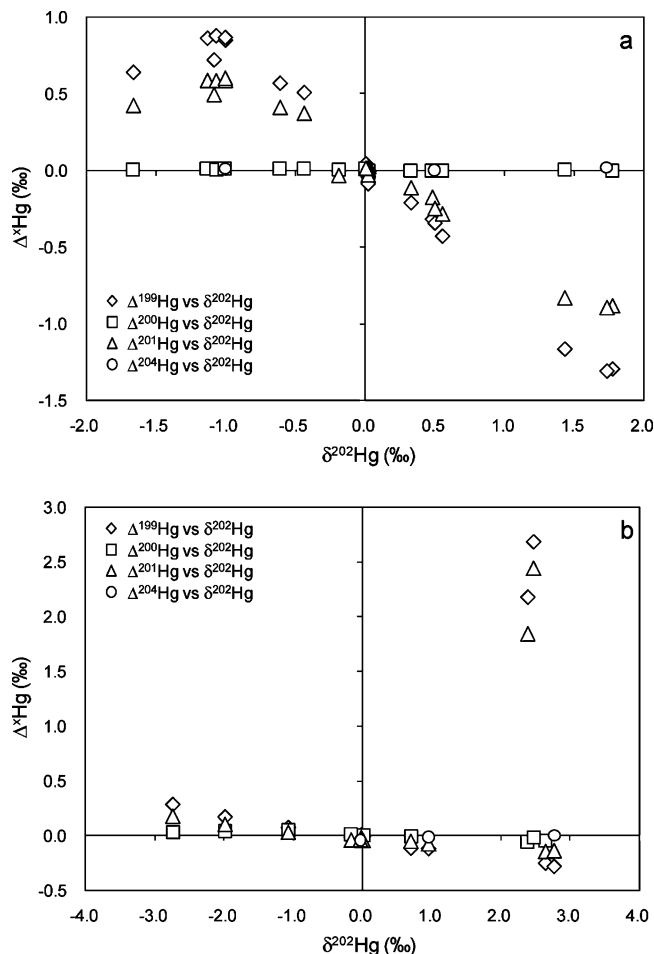


Figure 3. $\Delta^x\text{Hg}$ ($x = 199, 200, 201,$ and 204) against $\delta^{202}\text{Hg}$ for cysteine (a) and serine (b). Data points with positive $\delta^{202}\text{Hg}$ are samples of reactant and those with negative $\delta^{202}\text{Hg}$ are samples from product. Some selected samples are measured twice to determine $\delta^{204}\text{Hg}$. Both measurements of these samples are individually plotted and showed reproducible isotope compositions. Positive $\Delta^x\text{Hg}$ values in the upper right quadrant of (b) represent Hg(II) samples collected at 4 and 6 h.

Hg (mass dependent or magnetic isotope effects) previously reported in most other kinetic processes.^{28,36,39,50–54} Please note that the δ value is the net isotope fractionation consisting of the contributions of all concurrent isotope effects. Then, the anomalous isotope effect causing depletion of ^{199}Hg in the reactant must be much more dominant than the concurrent opposite mass dependent isotope effects to exhibit an overall negative $\delta^{199}\text{Hg}$ in the reactant.

More evidence for this anomalous isotope effect is illustrated in Figure 3a, showing $\Delta^x\text{Hg}$ against $\delta^{202}\text{Hg}$ during reduction by cysteine. According to their $\Delta^x\text{Hg}$ values, no isotopic anomalies were detected for nonmagnetic isotope pairs $^{200}\text{Hg}/^{198}\text{Hg}$ and $^{204}\text{Hg}/^{198}\text{Hg}$, suggesting the dominant MIF only operates on magnetic isotopes. It is clear that both magnetic isotopes, ^{199}Hg and ^{201}Hg , are subject to the same MIF, because $\Delta^{199}\text{Hg}$ and $\Delta^{201}\text{Hg}$ are both negative in the reactant and positive in the product. The $\Delta^{199}\text{Hg}/\Delta^{201}\text{Hg}$ slope obtained from the linear regression of all $\Delta^{199}\text{Hg}$ vs $\Delta^{201}\text{Hg}$ is 1.46 ± 0.03 (2SE, $r^2 = 0.998$, $P < 0.0001$), which is between the slopes previously determined for photochemical reduction by natural DOM and nonphotochemical reduction.^{28,36,40}

Therefore, this anomalous isotope effect during photochemical reduction of Hg(II) by cysteine resulted in specific enrichment of magnetic isotopes in the product Hg(0) , which is a sign of

MIE, but its direction is opposite the MIE previously observed for the photochemical reduction of Hg(II) by natural DOM. The other mass independent isotope effect, NFS, may contribute to but not completely account for $\Delta^{199}\text{Hg}$ and $\Delta^{201}\text{Hg}$ observed in this experiment. NFS also produces negative $\Delta^{199}\text{Hg}$ and $\Delta^{201}\text{Hg}$ in the reactant due to the odd–even staggering of nuclear charge radii, but it would enrich heavier/larger isotopes in the reactant and thus would not produce negative $\delta^{199}\text{Hg}$.^{38,40} Therefore, NFS is not the dominant isotope effect in this reduction.

For simplicity, the known MIE that enriches magnetic isotopes in initial reactants will be referred to as (+)MIE and the reversed one observed here as (–)MIE in the following text.

3.1.3. Isotope Fractionation during Photochemical Reduction by Serine. The dominant isotope effect during photochemical reduction by serine showed a clear change over time. At 0, 1, and 2 h (corresponding to $f_R = 1.00, 0.67,$ and 0.21 , respectively), the mass independent isotope effect is dominated by NFS. As demonstrated by Figure 2b and Figure 3b, both $\delta^{199}\text{Hg}$ and $\delta^{202}\text{Hg}$ comply with Rayleigh models in this stage of the reaction. Negative $\Delta^{199}\text{Hg}$ and $\Delta^{201}\text{Hg}$ but positive $\delta^{199}\text{Hg}$ and $\delta^{201}\text{Hg}$ were produced in the reactant. As already pointed out, this is a clear sign of NFS. The fractionation factors calculated with δ values of subsamples collected at 0, 1, and 2 h (Table 1) also showed the characteristic odd–even staggering of NFS, similar to those determined during abiotic nonphotochemical reduction of Hg(II) .⁴⁰ However, at 4 and 6 h, when the concentration of Hg(II) decreased to 1.5 nM or less (<1% of the initial Hg(II)), the isotope fractionation showed a distinct pattern of (+)MIE, characterized by the high and positive isotope anomalies for magnetic isotopes, $\Delta^{199}\text{Hg}$ and $\Delta^{201}\text{Hg}$, in the reactant. Please note the complementary Δ values are not detected in the product because >99% of initial Hg(II) had already been transferred to the product after 4 h, and the small increment of subsequently reduced Hg will not cause measurable addition of isotopic anomalies in the product. Although these low-concentration samples are subject to higher analytical uncertainties, Almadén standards measured at the same concentration did not show any significant isotopic anomalies. Therefore, we believe the detected $\Delta^{199}\text{Hg}$ and $\Delta^{201}\text{Hg}$ reflects in fact the true isotopic anomalies of samples rather than analytical artifacts. The change in the dominant isotope effect during the reduction process echoed the suppression of reduction rate toward the end of experiment and may suggest a change in the reaction mechanism.

The $\Delta^{199}\text{Hg}/\Delta^{201}\text{Hg}$ slope obtained from the linear regression of samples at 0, 1, and 2 h is 1.67 ± 0.28 (2SE, $r^2 = 0.936$, $P < 0.0001$), which is slightly higher than typical slopes determined for NFS (1.59–1.62).⁴⁰ The individual $\Delta^{199}\text{Hg}/\Delta^{201}\text{Hg}$ ratios for samples at 4 and 6 h are 1.18 and 1.10, respectively, and fall in the range determined for (+)MIE during photochemical reduction by natural DOM.^{28,36}

3.2. Photochemical Reduction by 12 Different LMWOC (Screening Experiment). **3.2.1. Extent of Reduction.** The extent of photochemical reduction of Hg(II) by 12 LMWOC is presented using the fraction of Hg in the residual reactant (f_R) and accumulated product (f_P) (Table 2). The mass balance of Hg (the sum of the three fractions of Hg in Table 2) in some of the experiments is relatively low. For example, for glycine it is only 0.68. This is probably caused by permeation of elemental Hg(0) through the wall of Teflon containers.⁵⁵ Therefore, f_R is considered to provide more accurate descriptions than f_P in these experiments.

In general, S-containing LMWOC resulted in notably less photochemical reduction than ligands without sulfur after the

TABLE 2: Extent and Isotope Fractionation of Photochemical Reduction of Hg(II) by 12 LMWOC (Screening Experiment)^a

	LMWOC	f_R	f_P	f_D	reactant Hg(II)					product Hg(0)				
					$\delta^{199}\text{Hg}$	$\delta^{201}\text{Hg}$	$\delta^{202}\text{Hg}$	$\Delta^{199}\text{Hg}$	$\Delta^{201}\text{Hg}$	$\delta^{199}\text{Hg}$	$\delta^{201}\text{Hg}$	$\delta^{202}\text{Hg}$	$\Delta^{199}\text{Hg}$	$\Delta^{201}\text{Hg}$
sulfurless	oxalic acid	0.11	0.59	0.04	3.53	3.42	0.94	3.30	2.71	-1.72	-2.18	-1.20	-1.42	-1.28
	glycolic acid	0.09	0.62	0.02	1.74	1.81	0.86	1.53	1.16	-0.81	-1.36	-1.25	-0.50	-0.42
	glycine	0.12	0.54	0.02	1.31	1.50	0.86	1.09	0.85	-1.06	-1.61	-1.40	-0.71	-0.56
	ethylene glycol	0.24	0.58	0.03	2.64	2.83	1.24	2.33	1.90	-1.64	-2.05	-1.31	-1.31	-1.07
	serine	0.14	0.73		3.09	3.36	1.13	2.80	2.51	-1.62	-1.88	-0.83	-1.41	-1.26
	ethylenediamine	0.49	0.28	0.07	0.07	0.42	0.64	-0.09	-0.07	0.24	-0.61	-1.59	0.64	0.58
	EDTA	0.82	0.08	0.01	0.69	0.80	0.31	0.61	0.56	-6.05	-6.47	-1.53	-5.67	-5.32
S-containing	methionine	0.55	0.15	0.08	-0.23	0.03	0.43	-0.34	-0.30	1.46	0.35	-1.80	1.91	1.71
	thiourea	0.56	0.14	0.02	-0.33	-0.19	0.23	-0.39	-0.36	1.59	0.54	-1.74	2.03	1.85
	cysteamine	0.71	0.40	0.01	-0.07	0.09	0.35	-0.16	-0.17	0.40	-0.30	-1.20	0.70	0.60
	L-cysteine-1	0.84	0.24	0.01	-0.09	0.25	0.53	-0.22	-0.15	0.44	-0.72	-1.76	0.88	0.60
	L-cysteine-2	0.93	0.21		-0.19	-0.03	0.15	-0.23	-0.15	0.70	-0.35	-1.49	1.08	0.78
	glutathione	0.70	0.36		-1.54	-0.80	0.69	-1.71	-1.32	2.73	1.41	-1.38	3.08	2.45

^a f_R , f_P , and f_D are the fraction of residual reactant Hg(II), fraction of accumulated product Hg(0) reduced in light conditions, and the fraction of Hg reduced in dark conditions, respectively. All δ and Δ values are in ‰.

same period of time, which is consistent with the reduction kinetics of the time-series experiment. S-containing LMWOC form stronger complexes with Hg(II) via reduced sulfur functional groups, such as -SH, -S-, and =S, making them less susceptible to photochemical reduction. Two sulfurless LMWOC, ethylenediamine and EDTA, also have high f_R . Ethylenediamine and EDTA are known for their chelating ability toward metal ions.^{56,57} Hg(II) is likely stabilized through formation of multidentate complexes. Reduction by serine and cysteine in the screening experiments seem to be slower than observed in the time-series experiment, which may be a result of lower concentrations of LMWOC and the Teflon container used, which is generally less efficient for UV transmission compared to quartz.

3.2.2. Isotope Fractionation. The pattern of isotope fractionation in the screening experiment echoed that of the time-series experiment (Table 2). Opposite magnetic isotope effects were determined for the two classes of LMWOC. First, all S-containing ligands resulted in negative isotope anomalies for magnetic isotopes, $\Delta^{199}\text{Hg}$ and $\Delta^{201}\text{Hg}$, as well as negative $\delta^{199}\text{Hg}$ in the reactant. This pattern is exactly the same as the (-)MIE determined for the time-series reduction by cysteine, suggesting that (-)MIE is the common isotope effect that is primarily induced by the photochemical reduction of Hg(II) bound to reduced S.

On the other hand, all sulfurless ligands (except ethylenediamine) led to enrichment of magnetic isotopes in the reactant (positive $\Delta^{199}\text{Hg}$ and $\Delta^{201}\text{Hg}$ in the reactant), implying that (+)MIE was the dominant MIF effect. This is consistent with samples collected after 4 h in the time-series reduction by serine. Ethylenediamine seems to be an exception. The MIF during photochemical reduction by ethylenediamine tends to enrich magnetic isotopes in the product (positive $\Delta^{199}\text{Hg}$ and $\Delta^{201}\text{Hg}$ in the product), suggesting a predominance of NFS or (-)MIE.

Linear relationships between $\Delta^{199}\text{Hg}$ and $\Delta^{201}\text{Hg}$ of the same type of LMWOC were also found in the screening experiment. For sulfurless ligands, the slope $\Delta^{199}\text{Hg}/\Delta^{201}\text{Hg} = 1.12 \pm 0.04$ (2SE, $r^2 = 0.996$, $P < 0.0001$), which is within the range of typical (+)MIE slopes and similar to the individual ratios of samples obtained after 4 h in the time-series experiment with serine. For S-containing ligands, $\Delta^{199}\text{Hg}/\Delta^{201}\text{Hg} = 1.21 \pm 0.07$ (2SE, $r^2 = 0.993$, $P < 0.0001$), lower than the slope determined for the time-series experiment with cysteine. Some degree of variation in slopes is not unexpected considering that several competing processes (i.e., hyperfine coupling, spin-orbital coupling and cage escape)⁴⁴ contribute to the overall Δ value

of MIE. Changes in the relative rates of these competing processes would change $\Delta^{199}\text{Hg}$ and $\Delta^{201}\text{Hg}$ to different degrees and therefore result in the variation of their ratio. Also, the slope of the time-series study is obtained from a consistent set of Δ values determined in a single experiment, while the slope of the screening experiment is composed of the linear regression of the final Δ values obtained from photoreduction experiments with several different organic compounds in individual reactions, with different degrees of reduction and isotope fractionation.

4. Discussion

4.1. Reversed Magnetic Isotope Effect. MIE was observed in the photochemical reduction of Hg(II) by both classes of LMWOC, but with different directions, which actually depends on the initial spin multiplicity of the paramagnetic intermediates of spin-selective reactions.^{41,58} So far, (+)MIE has been identified for various elements such as C, O, S, Si, Ge,⁵⁹ Hg,⁶⁰ and U,⁶¹ and is almost exclusively explained through radical pair mechanism according to the following scenario: when a molecule R-R' is excited from its ground singlet state (S_0) to a higher singlet state (e.g., S_1), it can undergo a rapid intersystem crossing (ISC) to the closest triplet state (T_1), and then dissociate to a triplet radical pair³[R[•],R'[•]], which is temporarily trapped in a solvent cage. The fate of this triplet radical pair is spin selective. Radicals centered with magnetic isotopes can induce fast triplet-singlet ISC by hyperfine coupling (HFC). As a result, radical pairs centered with magnetic isotopes have a higher probability to recombine than those centered with nonmagnetic isotopes, leading to selective enrichment of magnetic isotopes in the initial reactant.

An important premise of this scenario is that radical pairs are generated in triplet states. However, photoinduced bond dissociation may occur through either singlet or triplet channels depending on the nature of bonds and reaction conditions, such as temperature and wavelength.⁶²⁻⁶⁶ Photolysis through the singlet channel is usually inhibited by the spin-permitted recombination of singlet geminate radical pairs, which readily regenerate the initial reactants. However, in the presence of magnetic isotopes, HFC can induce ISC from singlet to triplet radical pairs, which are now spin-forbidden to recombine and thus decay to products that are enriched with magnetic isotopes. A schematic diagram of this spin-selective mechanism is shown in Figure 4. This mechanism has been proposed to be the underlying cause of (-)MIE. It was best demonstrated by thermal reactions, which produce radical pairs that are born in singlet states,^{47,48,58,67} but was also observed during photolysis.^{41,46}

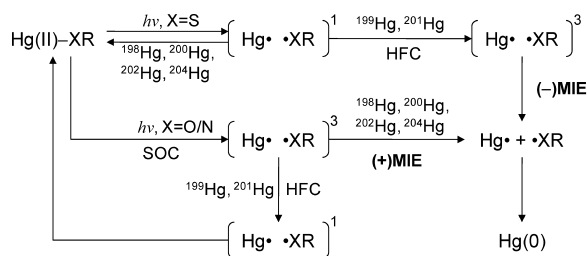


Figure 4. Schematic diagram of the mechanisms of (+)MIE and (-)MIE for a simplified generalized Hg(II)–XR complex, where XR represents reduced sulfur or O/N donor groups of LMWOC. The superscript “1” represents singlet excited states, and “3” represents triplet excited states. HFC and SOC stand for hyperfine coupling and spin–orbital coupling, respectively.

Therefore, the net MIE observed in our photochemical reduction experiments is likely a combination of both (+)MIE and (-)MIE, depending on which spin multiplicity dominates the initial radical intermediates. Dominance of (+)MIE during reduction by sulfurless LMWOC suggests these ligands tend to induce photolysis via triplet excited states, which are converted from singlet states as a result of ISC. S-containing LMWOC exclusively exhibited (-)MIE, suggesting that photolysis directly from singlet excited states is favored by these ligands (Figure 4). ISC from an excited singlet state to its corresponding triplet state is usually enhanced by the presence of heavy atoms such as Hg, due to their strong spin–orbital coupling (SOC) effect. Substitution of oxygen with sulfur in a Hg–XR bond should increase the rate of ISC due to the heavy atom effect, and therefore, increase the probability of photolysis via triplet excited states. However, our results revealed the opposite. A tentative explanation is that the singlet–triplet energy gap increases when an O-donor ligand is substituted by an S-donor ligand, which may delay the intramolecular singlet–triplet ISC after excitation. However, this mechanism needs further investigation.

As photolysis via singlet excited states is suppressed by the spin-permitted back-reaction, it is conceivable that photochemical reduction dominated by this mechanism is slower than those dominated by photolysis from triplet excited states. This could account to a certain degree for the slower reduction of Hg(II) by S-containing LMWOC observed in our experiments.

4.2. Mechanisms of Photochemical Reduction of Hg(II) by LMWOC. The dependence of isotope fractionation on reaction pathways is well recognized. The diverse mass independent isotope effects observed in this study are directly linked to various mechanisms of photochemical reduction of Hg(II) by LMWOC.

The photochemistry of dissolved Hg(II) induced by low wavelength irradiation ($\lambda < 300$ nm) has been characterized in some detail by absorption spectroscopy. Hg(II) complexes such as Hg(II)–halides and Hg(II)–C absorb energy in the long-wavelength UV range by ligand to metal charge transfer (LMCT) excitation. The 6s orbital of Hg(II) is assumed to be the acceptor orbital.^{3,68,69} The LMCT type photolysis leads to the formation of Hg(I) and ligand radicals (R[•]). Hg(I) may recombine to form Hg₂²⁺, which undergoes a homolysis of the metal–metal bond by $\sigma\sigma^*$ excitation, leading to a Hg⁺ radical, which is highly reactive and readily scavenged by electron donors such as alcohols to give elemental Hg.^{70,71} With natural sunlight, photolytic cleavage of Hg–R bonds is also suggested to be the main mechanism of Hg(II) reduction in natural waters.¹⁰ However, secondary reduction by reactive intermediates produced by primary photochemical processes, such as

HCOO[•], HO₂[•]/O₂⁻ and [•]CH₃, is also proposed to be responsible for Hg(II) reduction in the presence of LMWOC.⁷

The discovery of mass independent isotope effects (MIE and NFS) can provide more insights to the mechanism of photochemical reduction of Hg(II). MIE was detected for both classes of LMWOC, suggesting intermediate radical pairs that involve Hg are consistently produced by all LMWOC. Since Hg(II) is known to coordinate to O, N, and S donor functional groups,^{72,73} radical pairs are most likely generated from homolytic cleavage of a Hg–XR bond (X = S, O, and N), which should be the primary photochemical procedure of Hg(II) reduction. This is the only known mechanism that involves a spin selective process causing isotope fractionation. The energy required to break different Hg(II)–LMWOC bonds varies according to their binding strength, leading to different reduction rates. Also, different radical pairs are generated, which bear different hyperfine coupling constants that determine the rate of ISC. This could account for the variation in the degree of MIE. Furthermore, the sign of MIE may distinguish between singlet and triplet photolysis pathways, as discussed earlier.

A shift of the dominant isotope effect was observed during the time-series reduction by serine. NFS dominates in the early stage of this reaction. This may suggest that the photochemical reduction is not necessarily governed by direct photolysis of Hg–O/N donor bonds, at least not in the early stage of this process. Instead, secondary reduction by radicals such as CO₂^{-•} and [•]COOH generated from the carboxyl group of serine may be more significant. Unlike the direct photolysis, this mechanism does not generate radical pairs and thus does not induce MIE, but it is subject to NFS because electron transfer occurs at the 6s orbital. The lack of MIE in photochemical reduction was also observed in UV reduction of Hg(II) by formic acid performed by Yang and Sturgeon.⁵⁴ Their study found minor MIF with the characteristics of NFS, which could be explained by the dominance of secondary reduction. It is also worth noting that MIE started to show during the later stage of the reduction by serine. This indicates that direct photolysis started to outcompete secondary reduction when the concentration of Hg(II) decreased.

Therefore, both direct photolysis of Hg–LMWOC bonds and secondary reduction are possible mechanisms of photochemical reduction of Hg(II). They can be discerned by specific mass independent isotope effects. The overall isotope effect depends on which mechanism is prevailing.

4.3. Comparison between Natural DOM and LMWOC Using Isotope Effects. One purpose of this study is to unveil the isotope effects caused by specific binding sites of natural DOM. Although this study did not attempt to exactly reproduce environmental conditions, Hg(II) reduction rates measured in the presence of serine are comparable to rate constants reported for photochemical reduction observed in natural waters samples (0.2–1.0 h⁻¹).^{1,74,75} In contrast, the rate constant generated by cysteine is almost 1 order of magnitude lower. This would suggest that Hg(0) in natural waters primarily originates from Hg(II) bound to O/N donor groups in DOM.

Isotope effects provide further evidence for the reactivity of Hg(II). One important difference between the reduction by natural DOM and LMWOC is that no (-)MIE was determined for natural DOM in contrast to results with S-containing LMWOC presented here. This also suggests that, although Hg(II) is mainly bound to reduced S functional groups of DOM in natural waters according to equilibrium models,¹⁸ the majority of Hg(0) is actually produced from species that bind to O/N donor groups of DOM. Zheng and Hintelmann³⁶ suggested the

presence of multiple pools of Hg(II) with different reactivity due to their binding conditions and found ~10–20% of Hg(II) was still easily reducible even at very low Hg/DOC ratios. It is very likely that Hg(II) may bind to some O/N groups even when the reduced S groups are in excess of Hg(II) because of the high abundance of O/N groups in natural DOM.¹¹ This is a major difference between natural DOM and LMWOC. In DOM, O/N groups are always much more abundant than reduced S groups, while in S-containing LMWOC, reduced S groups are often the only binding site for Hg at low Hg/LMWOC ratios. Moreover, the disequilibrium of the complexation between Hg(II) and DOM may also result in temporary dominance of Hg–O/N species in natural waters.⁷⁶ Therefore, it is possible that initially the photochemical reduction of Hg(II) by natural DOM is dominated by the photolysis of Hg–O/N bonds, which generated (+)MIE corresponding to sulfurless LMWOC. As the reduction progresses and the photolysis of Hg–S bonds starts to prevail, (–)MIE may occur but is overshadowed by prior isotope enrichment through (+)MIE. In addition, (–)MIE was likely low as a result of slow reduction of Hg(II) associated with reduced S groups.

A variation of isotope fractionation during Hg(II) photochemical reduction by natural DOM was previously observed with Hg/DOC ratios: (+)MIE decreased gradually as Hg/DOC decreased, but it was significantly suppressed at the highest Hg/DOC ratio.³⁶ Now we may explain this variation by the isotope effects determined for LMWOC in this study. With the decrease of Hg/DOC, there is less Hg(II) that binds to O/N binding sites, which generates less (+)MIE. The increasing Hg–S either does not fractionate (not reduced) or produces (–)MIE that counteracts the (+)MIE produced by O/N binding sites. Therefore, the overall (+)MIE decreases with decreasing Hg/DOC. With increasing Hg/DOC, secondary reduction mechanism may play a larger role because of the increasing Hg–O/N, which was shown to be readily reduced by free radicals in the time-series reduction by serine. Therefore, the increase of secondary reduction would enhance NFS and suppress (+)MIE at very high Hg/DOC ratios.

5. Conclusions

Photochemical reduction of Hg(II) by two classes of LMWOC yielded dramatically different results. Cysteine, an S-containing compound, exhibited a relatively slow pseudo-first-order reduction with a rate constant of 0.047 h⁻¹. Serine, a sulfurless compound, resulted in a much faster reduction of Hg(II) with an initial rate constant of 0.640 h⁻¹. Significant but different mass independent isotope fractionation was observed during reduction by both compounds. MIF caused by cysteine is dominated by a reversed magnetic isotope effect ((–)MIE), which tends to deplete magnetic isotopes (¹⁹⁹Hg and ²⁰¹Hg) from the reactant Hg(II) phase and enrich them in the product Hg(0). Contrarily, MIF caused by serine followed the pattern of NFS initially and exhibited the (+)MIE pattern as the concentration of Hg(II) decreased. These clear differences between cysteine and serine were reproduced by experiments with 12 different LMWOC, suggesting these differences are not limited to specific compounds but have more general implications for LMWOC with and without reduced sulfur groups.

The sign of MIE indicates opposite initial spin multiplicity of the intermediate radical pairs, and hence, different photolysis pathways, during photochemical reduction. We believe this important difference is related to the fundamental nature of bonds between Hg(II) and O/N or reduced S donor groups. However, more research is required to clarify why photolysis

via a singlet excited state that is generally higher in energy than the corresponding triplet state is more pronounced for reduced S groups than for O/N groups.

The MIF signature allows us to distinguish between different mechanisms of photochemical reduction and can serve as an indicator for the reactivity of Hg(II) species under different binding conditions. Primary photolysis and secondary photochemical reduction are both found to be probable pathways. Both mechanisms likely control the net reduction rate and isotope fractionation. The comparison between the LMWOC and natural DOM in terms of mass independent isotope effects suggests that the main photoreducible Hg(II) species in natural waters are those that bind to O/N donor groups rather than to reduced S groups of DOM, and the total isotope effects observed for bulk DOM are actually the combination of specific isotope effects induced by different functional groups.

Acknowledgment. We thank the two reviewers for their insightful suggestions. We also thank Dr. Bridget Bergquist, Dr. Dirk Wallschläger, and Dr. David Ellis for providing their thoughts on this study. The Suntest XLS+ is provided by Dr. Peter Dillon.

References and Notes

- (1) Poulain, A. J.; Amyot, M.; Findlay, D.; Telor, S.; Barkay, T.; Hintelmann, H. *Limnol. Oceanogr.* **2004**, *49*, 2265.
- (2) Gardfeldt, K.; Jonsson, M. *J. Phys. Chem. A* **2003**, *107*, 4478.
- (3) Kunkely, H.; Horvath, O.; Vogler, A. *Coord. Chem. Rev.* **1997**, *159*, 85.
- (4) Xiao, Z. F.; Stromberg, D.; Lindqvist, O. *Water, Air, Soil Pollut.* **1995**, *80*, 789.
- (5) Deng, L.; Fu, D. F.; Deng, N. S. *J. Hazard. Mater.* **2009**, *164*, 798.
- (6) Deng, L.; Wu, F.; Deng, N. S.; Zuo, Y. G. *J. Photochem. Photobiol., B* **2008**, *91*, 117.
- (7) Pehkonen, S. O.; Lin, C. J. *J. Air Waste Manage. Assoc.* **1998**, *48*, 144.
- (8) Zhang, H.; Lindberg, S. E. *Environ. Sci. Technol.* **2001**, *35*, 928.
- (9) Nriagu, J. O. *Sci. Total Environ.* **1994**, *154*, 1.
- (10) Zhang, H. Photochemical redox reactions of mercury. *Recent Developments in Mercury Science* **2006**, *120*, 37.
- (11) Hesterberg, D.; Chou, J. W.; Hutchison, K. J.; Sayers, D. E. *Environ. Sci. Technol.* **2001**, *35*, 2741.
- (12) Qian, J.; Skyllberg, U.; Frech, W.; Bleam, W. F.; Bloom, P. R.; Petit, P. E. *Geochim. Cosmochim. Acta* **2002**, *66*, 3873.
- (13) Xia, K.; Skyllberg, U. L.; Bleam, W. F.; Bloom, P. R.; Nater, E. A.; Helmke, P. A. *Environ. Sci. Technol.* **1999**, *33*, 257.
- (14) Amon, R. M. W.; Benner, R. *Nature* **1994**, *369*, 549.
- (15) Benner, R.; Pakulski, J. D.; McCarthy, M.; Hedges, J. I.; Hatcher, P. G. *Science* **1992**, *255*, 1561.
- (16) Benoit, J. M.; Mason, R. P.; Gilmour, C. C.; Aiken, G. R. *Geochim. Cosmochim. Acta* **2001**, *65*, 4445.
- (17) Drexler, R. T.; Haitzer, M.; Ryan, J. N.; Aiken, G. R.; Nagy, K. L. *Environ. Sci. Technol.* **2002**, *36*, 4058.
- (18) Haitzer, M.; Aiken, G. R.; Ryan, J. N. *Environ. Sci. Technol.* **2002**, *36*, 3564.
- (19) Hsu, H.; Sedlak, D. L. *Environ. Sci. Technol.* **2003**, *37*, 2743.
- (20) Allard, B.; Boren, H.; Pettersson, C.; Zhang, G. *Environ. Int.* **1994**, *20*, 97.
- (21) Brinkmann, T.; Horsch, P.; Sartorius, D.; Frimmel, F. H. *Environ. Sci. Technol.* **2003**, *37*, 4190.
- (22) Moran, M. A.; Zepp, R. G. *Limnol. Oceanogr.* **1997**, *42*, 1307.
- (23) Zhou, X. L.; Mopper, K. *Mar. Chem.* **1997**, *56*, 201.
- (24) Han, C. F.; Zheng, C. B.; Wang, J.; Cheng, G. L.; Lv, Y.; Hou, X. D. *Anal. Bioanal. Chem.* **2007**, *388*, 825.
- (25) He, Y. H.; Hou, X. D.; Zheng, C. B.; Sturgeon, R. E. *Anal. Bioanal. Chem.* **2007**, *388*, 769.
- (26) Wu, L.; Zheng, C. B.; Ma, Q.; Hu, C. W.; Hou, X. *Appl. Spectrosc. Rev.* **2007**, *42*, 79.
- (27) Yin, Y. M.; Qiu, J. H.; Yang, L. M.; Wang, Q. Q. *Anal. Bioanal. Chem.* **2007**, *388*, 831.
- (28) Bergquist, B. A.; Blum, J. D. *Science* **2007**, *318*, 417.
- (29) Biswas, A.; Blum, J. D.; Bergquist, B. A.; Keeler, G. J.; Xie, Z. Q. *Environ. Sci. Technol.* **2008**, *42*, 8303.
- (30) Carignan, J.; Estrade, N.; Sonke, J. E.; Donard, O. F. X. *Environ. Sci. Technol.* **2009**, *43*, 5660.

- (31) Ghosh, S.; Xu, Y. F.; Humayun, M.; Odom, L. *Geochem. Geophys. Geosyst.* **2008**, *9*, Q03004 Doi 10.1029/2007gc001827.
- (32) Jackson, T. A.; Whittle, D. M.; Evans, M. S.; Muir, D. C. G. *Appl. Geochem.* **2008**, *23*, 547.
- (33) Sherman, L. S.; Blum, J. D.; Nordstrom, D. K.; McCleskey, R. B.; Barkay, T.; Vetriani, C. *Earth Planet. Sci. Lett.* **2009**, *279*, 86.
- (34) Stetson, S. J.; Gray, J. E.; Wanty, R. B.; Macalady, D. L. *Environ. Sci. Technol.* **2009**, *43*, 7331.
- (35) Zambardi, T.; Sonke, J. E.; Toutain, J. P.; Sortino, F.; Shinohara, H. *Earth Planet. Sci. Lett.* **2009**, *277*, 236.
- (36) Zheng, W.; Hintelmann, H. *Geochim. Cosmochim. Acta* **2009**, *73*, 6704.
- (37) Bigeleisen, J. *J. Am. Chem. Soc.* **1996**, *118*, 3676.
- (38) Schauble, E. A. *Geochim. Cosmochim. Acta* **2007**, *71*, 2170.
- (39) Estrade, N.; Carignan, J.; Sonke, J. E.; Donard, O. F. X. *Geochim. Cosmochim. Acta* **2009**, *73*, 2693.
- (40) Zheng, W.; Hintelmann, H. *J. Phys. Chem. A*, DOI 10.1021/jp910353y.
- (41) Buchachenko, A. L. *J. Phys. Chem. A* **2001**, *105*, 9995.
- (42) Turro, N. J. *Proc. Natl. Acad. Sci. U.S.A.* **1983**, *80*, 609.
- (43) Buchachenko, A. L. *Russ. Chem. Rev.* **2009**, *78*, 319.
- (44) Steiner, U. E.; Ulrich, T. *Chem. Rev.* **1989**, *89*, 51.
- (45) Turro, N. J.; Kraeutler, B. *Acc. Chem. Res.* **1980**, *13*, 369.
- (46) Buchachenko, A. L.; Ivanov, V. L.; Roznyatovskii, V. A.; Vorob'ev, A. K.; Ustynyuk, Y. A. *Dokl. Phys. Chem.* **2008**, *420*, 85.
- (47) Buchachenko, A. L.; Kouznetsov, D. A.; Breslavskaya, N. N.; Orlova, M. A. *J. Phys. Chem. B* **2008**, *112*, 2548.
- (48) Buchachenko, A. L.; Kouznetsov, D. A.; Shishkov, A. V. *J. Phys. Chem. A* **2004**, *108*, 707.
- (49) Step, E. N.; Tarasov, V. F.; Buchachenko, A. L. *Bull. Acad. Sci. USSR Div. Chem. Sci.* **1988**, *37*, 2024.
- (50) Zheng, W.; Foucher, D.; Hintelmann, H. *J. Anal. At. Spectrom.* **2007**, *22*, 1097.
- (51) Kritee, K.; Barkay, T.; Blum, J. D. *Geochim. Cosmochim. Acta* **2009**, *73*, 1285.
- (52) Kritee, K.; Blum, J. D.; Barkay, T. *Environ. Sci. Technol.* **2008**, *42*, 9171.
- (53) Kritee, K.; Blum, J. D.; Johnson, M. W.; Bergquist, B. A.; Barkay, T. *Environ. Sci. Technol.* **2007**, *41*, 1889.
- (54) Yang, L.; Sturgeon, R. *Anal. Bioanal. Chem.* **2009**, *393*, 377.
- (55) Hall, G. E. M.; Pelchat, J. C.; Pelchat, P.; Vaive, J. E. *Analyst* **2002**, *127*, 674.
- (56) Douglas, B. E.; Radanovic, D. J. *Coord. Chem. Rev.* **1993**, *128*, 139.
- (57) Radanovic, D. J. *Coord. Chem. Rev.* **1984**, *54*, 159.
- (58) Buchachenko, A. L.; Kuznetsov, D. A. *Mol. Biol.* **2006**, *40*, 12.
- (59) Wakasa, M.; Hayashi, H.; Ohara, K.; Takada, T. *J. Am. Chem. Soc.* **1998**, *120*, 3227.
- (60) Buchachenko, A. L.; Ivanov, V. L.; Roznyatovskii, V. A.; Ar-tamkina, G. A.; Vorob'ev, A. K.; Ustynyuk, Y. A. *Dokl. Phys. Chem.* **2007**, *413*, 39.
- (61) Buchachenko, A. L.; Khudiyakov, I. V. *Acc. Chem. Res.* **1991**, *24*, 177.
- (62) Ivanov, V. L.; Roznyatovskii, V. A.; Ustynyuk, Y. A.; Buch-achenko, A. L. *Russ. J. Phys. Chem. A* **2008**, *82*, 119.
- (63) Kageyama, A.; Yashiro, H.; Murai, H. *Mol. Phys.* **2002**, *100*, 1341.
- (64) Pohlars, G.; Dreeskamp, H.; Grimme, S. *J. Photochem. Photobiol., A* **1996**, *95*, 41.
- (65) Step, E. N.; Tarasov, V. F.; Buchachenko, A. L. *Chem. Phys. Lett.* **1988**, *144*, 523.
- (66) Yamaji, M.; Inomata, S.; Nakajima, S.; Akiyama, K.; Tobita, S.; Marciniak, B. *J. Phys. Chem. A* **2005**, *109*, 3843.
- (67) Grissom, C. B. *Chem. Rev.* **1995**, *95*, 3.
- (68) Horvath, O.; Vogler, A. *Inorg. Chem.* **1993**, *32*, 5485.
- (69) Horvath, O.; Vogler, A. *Inorg. Chem. Commun.* **1998**, *1*, 270.
- (70) Horvath, O.; Miko, I. *J. Photochem. Photobiol., A* **1999**, *128*, 33.
- (71) Horvath, O.; Miko, I. *Inorg. Chem. Commun.* **1999**, *2*, 143.
- (72) Foti, C.; Giuffre, O.; Lando, G.; Sammartano, S. *J. Chem. Eng. Data* **2009**, *54*, 893.
- (73) Oram, P. D.; Fang, X. J.; Fernando, Q.; Letkeman, P.; Letkeman, D. *Chem. Res. Toxicol.* **1996**, *9*, 709.
- (74) O'Driscoll, N. J.; Siciliano, S. D.; Lean, D. R. S.; Amyot, M. *Environ. Sci. Technol.* **2006**, *40*, 837.
- (75) Qureshi, A.; O'Driscoll, N. J.; MacLeod, M.; Neuhold, Y. M.; Hungerbuhler, K. *Environ. Sci. Technol.* **2010**, *44*, 644.
- (76) Miller, C. L.; Southworth, G.; Brooks, S.; Liang, L.; Gu, B. *Environ. Sci. Technol.* **2009**, *43*, 8548.